# Computer Aided Diagnosis System for Pulmonary Nodules Using Hierarchical Feature Extraction


K. Takei
Grad. Sch. of Eng.
Tohoku Univ.
Sendai, Aoba
980-8579

N. Homma, T. Ishibashi
Faculty of Med.
Tohoku Univ.
Sendai, Seiryo-machi
980-8575

M. Sakai
Grad. Sch. of Info. Sci.
Tohoku Univ.
Sendai, Kawauchi
980-8576

M. Yoshizawa
Info. Syn. Center
Tohoku Univ.
Sendai, Aoba
980-8579

K. Abe
Col. of Eng.
Nihon Univ.
Koriyama, Tamura
963-8642



## Abstract

In this paper, we propose a new diagnosis method of pulmonary nodules in CT images to reduce false positive rate (FP) for a high true positive rate (TP) conditions. An essential core of the method is in its hierarchical feature extraction. In the 1st stage, novel orientation features of nodules in a small region of interest (ROI) are extracted in addition to several conventional features, while a more structural feature of a surrounding area of the ROI is extracted in the 2nd stage. Without the orientation features, when TP was 90%, FP was about 65% and 55% in the 1st and 2nd stage, respectively. On the other hand, using the orientation features, FP was about 15% and only 5% in the 1st and 2nd stages, respectively. These improvement of the discrimination rate clearly demonstrates the effectiveness of the proposed hierarchical method on the nodules diagnosis.


## 1 Introduction

With the increasing of the mortality rate for lung cancer, computed tomography (CT) has been used for detection of lung cancer at early stages [1]. However, using CT may exhaust for radiologists because CT generates a large number of images (over 30 per patient) and they must read all of them. Therefore, some computer-aided diagnosis (CAD) systems have been developed. Okumura et al. proposed a N-Quoit filter [2]. Lee et al. proposed a nodule detection system using a genetic algorithm [3]. However, although these CAD systems can automatically detect pulmonary nodules with a high true positive rate (TP), the false positive rate (FP) is also high. This is not appropriate for clinical use since such high FP may disturb radiologist's diagnosis process. To reduce FP, several methods have been proposed. Suzuki et al. proposed a massive training artificial neural network (MTANN) for reduction of FP [4]. Nakamura et al. proposed a nodule recognition system using subspace method [5].

In this paper, we propose a new method to diagnose pulmonary nodules in CT images. Especially, compared to the methods mentioned above, we aim to further reduce FP for a high TP conditions by extracting novel orientation and structural features of the nodules in a hierarchical manner.

## 2 Discrimination algorithm

The proposed method for discrimination between shadows of nodules and non-nodules mainly consists of 2 stages. In the first stage, nodule candidates are differentiated from the non-nodule ones using novel orientation features of a small size image of region of interest (ROI). On the other hand, in the second stage, a structural feature of surrounding area of the ROI is used for further discriminating the final nodule candidates from the nodule ones in the first stage.

### 2.1 Discrimination using orientation features of shadows

Orientation information can be very important to recognize shapes of subjects, but as we know, there is no CAD system using effective orientation features of nodules. To extracted the orientation features, we may use a gabor filter whose impulse response is defined by a harmonic function multiplied by a Gaussian function. Indeed, due to its orientation selectivity, the gabor filter has been applied to feature extraction problems for various image recognition systems, such as face recognition, fingerprint recognition and so on [6] [7].

#### 2.1.1 Feature extraction

In the first stage, to extract features for nodules and non-nodules recognition, we firstly binarized the

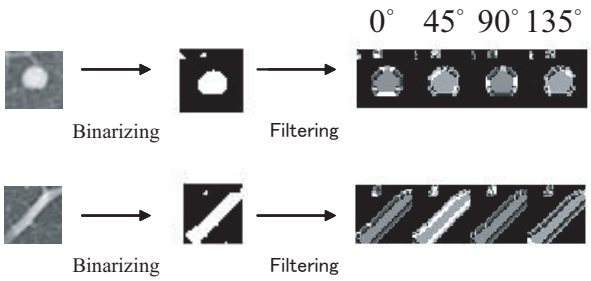


Figure 1: Examples of 4 orientaion features.

images in ROI. Then, we extracted $M_1$ orientation features from the binarized image by using the gabor filter given as

$$g(x, y, \sigma, \lambda, \gamma, \theta) = \exp\left(-\frac{x'^2 + \gamma^2 y'^2}{2\sigma^2}\right)\cos\left(\frac{2\pi x'}{\lambda}\right) \quad (1)$$

where $\theta$ is the angle of orientation, $\sigma$ is the bandwidth, $\gamma$ is the aspect ratio, and $\lambda$ is the wave length. $x'$ and $y'$ are, respectively, given by

$$x' = x\cos\theta + y\sin\theta, \qquad y' = -x\sin\theta + y\cos\theta \quad (2)$$

The orientation features are obtained from the convolution of the binarized image $I_\beta(x, y)$ of the original image $I(x, y)$ and $g(x, y, \sigma, \lambda, \gamma, \theta)$ given as

$$O(x, y) = I_\beta(x, y) * g(x, y, \sigma, \lambda, \gamma, \theta) \quad (3)$$

Figure 1 shows examples of filtered image of 4 orientaions. For the original binarized and each orientation images, we calculated three features (mean, variance, and entropy of intensity). Consequently, by adding $3 \times M_1$ features to the 3 original features, we got total $3 \times (1 + M_1)$ features of the binarized image. Then we defined a feature vector $X$ of $3 \times (1 + M_1)$ features, $X = [x_1, x_2, \cdots, x_{3(1+\mathrm{M}_1)}]^T$, of nodule or non-nodule image.

### 2.1.2 Clustering

Using $C_1$ dominant principal components of the feature vectors $X$ of training data, we made nodule and non-nodule clusters of the binarized images by $K$-means method [8]. The $K$-means method algorithm is implemented as

1. Initialize vectors of cluster centroids $\mu_1, \cdots, \mu_k$.
2. Classify each feature vector $X$ to the cluster $\hat{p}$ with the smallest distance

$$\hat{p} = \arg\min_{1 \le j \le k} D(X, \mu_j) \quad (4)$$

where $D(X, \mu_j)$ denotes the Euclidean distance of $X$ and $\mu_j$.

3. Based on the classification, update the cluster centroids as

$$\mu_j = \frac{1}{n_j}\sum_{i=1}^{n_j} X_i^{(j)} \quad (5)$$

where $n_j, j = 1, 2, \cdots, k$, are the numbers of nodules or non-nodules in clusters $j$, and $X_i^{(j)}$ are the $i$th feature vectors in cluster $j$.

4. If any clusters centroid is changed, go to step 2., otherwise stop the algorithm.

In determination of the number of clusters $k$, we employed the cluster validity analysis [8]. The cluster separation measure $\rho(k)$ is defined as

$$\rho(k) = \frac{1}{k-1}\sum_{i=1}^{k-1}\max_{i<j\le k}\left(\frac{\eta_i + \eta_j}{\xi_{ij}}\right) \quad (6)$$

where

$$\eta_j = \frac{1}{n_j}\sum_{i=1}^{n_j} D(X_i^{(j)}, \mu_j) \quad (7)$$

and

$$\xi_{ij} = D(\mu_i, \mu_j) \quad (8)$$

$\eta_j$ is the intra-cluster distance of cluster $j$, while $\xi_{ij}$ is the inter-cluster distance of clusters $i$ and $j$. The optimal number of clusters $\hat{k}$ is selected as

$$\hat{k} = \min_{1 \le k \le L} \rho(k) \quad (9)$$

In other words, the $K$-means algorithm is firstly tested for all candidates $k = 1, 2, \cdots, L$, and after that $k$ which gives the lowest value of $\rho(k)$ is chosen.

However, since $\rho(k)$ decreases as $L$ increases, it is not appropriate to determine the number of clusters by the minimum value of $\rho(k)$ simply. Therefore, in this paper, we employed the local minimum [9]. In other words, we determined $L$ when $\rho(L+1) - \rho(L)$ is maximum, and chose $\hat{k}$ which gives minimum value of $\rho(k)$, $k = 1, 2, \cdots, L$.

### 2.1.3 Determination of candidate clusters

Using the dominant $C_1$ principal components, we made, respectively, $P_1$ and $Q_1$ clusters of nodule and non-nodule images by the method in Section 2.1.2.

Then, we calculated Euclidean distances between test image and all the clusters. Let us consider $(P_1 + Q_1)$ distances $d^{A1}_{p_1}$, $p_1 = 1, 2, \cdots, P_1$, from $P_1$ nodule clusters and $d^{N1}_{q_1}$, $q_1 = 1, 2, \cdots, Q_1$, from $Q_1$ non-nodule ones. The discrimination in this first stage was conducted by comparing the minimum distances $d^{A1}_{p^*_1}$, $p^*_1 \in p_1$, from the nearest nodule cluster to the distances $d^{N1}_{q^*_1}$, $q^*_1 \in q_1$, from the non-nodule one. That is, if the ratio $d_1 = d^{A1}_{p^*_1}/d^{N1}_{q^*_1}$ is less than a threshold $\alpha_1$, then the test image can be a nodule candidate, otherwise a non-nodule one.

### 2.2 Discrimination using structural feature of shadows

In the second stage, we further discriminated the final nodule candidates from the nodule candidates in the first stage by using a structural feature of surrounding area of the ROI which includes nodule or non-nodule shadows. The reason why we pay attention to the surrounding feature is that there are differences between surrounding images of nodules and non-nodules as shown in Fig. 2. That is, even there is no big difference between nodule and non-nodule images in the small ROI, significant structural differences between surrounding areas of them can be found: The nodule tends to exist in isolation comparatively, while the non-nodule tends to exist with other shadows (vessel etc.).

To extract such structural feature, we used the fractal dimension of the surrounding area. The fractal dimension is a statistical quantity that gives an indication how completely a fractal appears to fill space. In fact, usefulness of the fractal dimension to quantify image structures has widely been reported in CAD systems [10][11]. The brief explanation of the algorithm in this second stage is as follow.

We binarized the surrounding images of shadows and calculated the three features of mean, variance and entropy by the same method as in the first stage. We also calculated the new feature of the fractal dimension using box counting algorithm [10][11]. For the original and $M_2$ orientation, i.e, $(1 + M_2)$ images, three and one new $(3 + 1 = 4)$ features are calculated. Consequently, we got total $4 \times (1 + M_2)$ features of the surrounding binarized image. Using dominant $C_2$ principal components of the $4 \times (1 + M_2)$ features of nodule and non-nodule training images, we made, respectively, $P_2$ nodule and $Q_2$ non-nodule clusters. Let us denote the minimum distance $d^{A2}_{p^*_2}$, $p^*_2 \in p_2 = 1, 2, \cdots, P_2$, from the nearest nodule cluster and $d^{N2}_{q^*_2}$, $q^*_2 \in q_2 = 1, 2, \cdots, Q_2$, from the nearest non-nodule cluster. If the ratio $d_2 = d^{A2}_{p^*_2}/d^{N2}_{q^*_2}$ is less than a threshold $\alpha_2$, then the test image can be a nodule, otherwise a non-nodule.

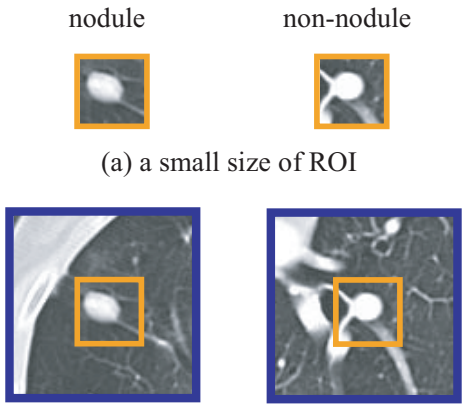


Figure 2: Examples of the surrounding images.

## 3 Experimental results

We used 97 nodule data (59 training image and 38 test image) and 174 non-nodule data (104 training image and 70 test image) from the database [12]. Image's size was $33 \times 33$ and $99 \times 99$ pixels in the first and second stages, respectively. Gabor filter's parameters $\sigma, \lambda$, and $\gamma$ were 1.5, 2.6 and 1, respectively. The numbers of clusters $P_i$ and $Q_i$, $i \in \{1, 2\}$, orientations $M_i$, principal components $C_i$ are shown in Table 1. The $M_i$ was determined empirically, and the $C_i$ was determined as the minimum value that satisfies the condition $\sum_{j=1}^{C_i} u_j > 0.95$ , where $u_j$ is the contribution ratio of principal component $j$.

Figure 3 shows the 4 receiver operating characteristic (ROC) curves by 4 different methods. Without 12

Table 1: Experimental conditions.

| Number of | 1st stage | 2nd stage |
|---|---|---|
| Nodule clusters | $P_1$=3 | $P_2$=2 |
| Non-nodule clusters | $Q_1$=15 | $Q_2$=3 |
| Orientations | $M_1$=4 | $M_2$=4 |
| Principal componets | $C_1$=5 | $C_2$=4 |

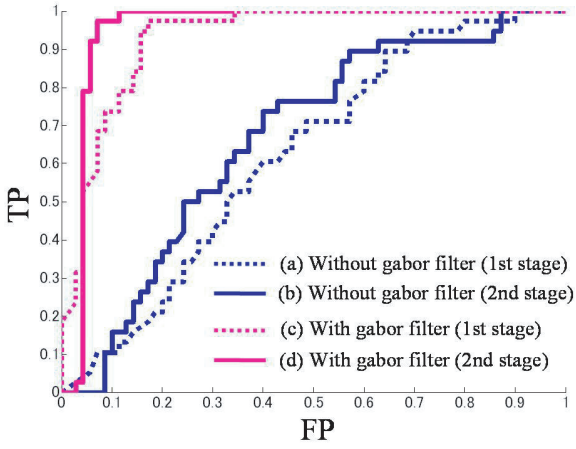


Figure 3: Comparison of ROC curves by using (a) conventional, (b) fractal, (c) orientation, and (d) orientation and fractal features.

features of 4 orientation outputs extracted by the gabor filter, FP was, respectively, about 65% and 55% in the first and second stages when TP was 90%. On the other hand, by using gabor filter, FP was about 15% (first stage) and 5% (second stage). The improvement of the discrimination rate, i.e, from 65% to 15% and from 55% to 5% in the first and second stages, respectively, clearly demonstrates effectiveness of the orientation and surrounding features on the pulmonary nodules diagnosis. In addition to this, FP was about 35% under the same condition by using a MTANN [4]. Although this rate can be improved if we could choose more suitable settings for the MTANN, we may claim that the discrimination rate of the proposed method is the same level or more than that of the MTANN.

## 4 Conclusion

We have proposed a new diagnosis method of pulmonary nodules in CT images. The results demonstrated that the proposed method can further reduce FP under a high TP condition compared to the conventional ones. This improvement has been achieved by extracting new orientation features of nodules in the small ROI using the gabor filter and by the hierarchical combination with the structural feature quantified by the fractal dimension of the larger area surrounding the ROI.

## References

[1] T. Iinuma et al.,"Preliminary specification of X-ray CT for lung cancer screening (LSCT) and its evaluation on risk-cost-effectiveness," *Nippon Acta Radiologica*, Vol. 52, pp.182-190, 1992. (in Japanese)

[2] T. Okumura et al., "Variable-N-Quoit fiter applied for automatic detection of lung cancer by X-ray CT," *Proc. of Computer-Assisted Radiology*, pp.242-247, 1998. (in Japanese)

[3] Y. Lee et al.,"Nodule detection on chest helical CT scans by using a genetic algorithm," *Proc. of IASTED International Conference on Intelligent Information Systems*, pp.67-70, 1997.

[4] K. Suzuki et al.,"Massive training artificial neural network (MTANN) for reduction of false-positives in computerized detection of lung nodules in low-dose computed tomography," *Med.Phys*, Vol. 30 (7), pp.1602-1617, 2003.

[5] Y. Nakamura et al., "Recognition of X-ray CT image using subspace method considering translation and rotation of pulmonary nodules," *TECHNICAL REPORT OF IEICE*, MI2004-102, pp.119-124, 2005. (in Japanese)

[6] K. C. Chung et al.,"Face recognition using principal component analysis of gabor filter responses," *Proceedings. International Workshop on 26-27 Sept* , pp.53-57, 1999.

[7] C. J. Lee et al.,"A Gabor filter-based approach to fingerprint recognition," *IEEE Workshop on 20-22 Oct*, Vol. 52, pp.371-378, 1999.

[8] C. W. Ngo et al.,"On clustering and retrieval of video shots through temporal slice analysis," *IEEE Trans. Mlt.*, Vol. 4, No.4 pp.446-458, 2002.

[9] S. Hattori et al.,"Video classification based on video description space," *TECHNICAL REPORT OF IEICE*, CS2003-150, pp. 55-60, 2003. (in Japanese)

[10] S. Kido et al.,"Fractal analysis of interstitial lung. abnormalities in chest radiography," *Radiographics*, Vol. 15, pp. 1457-1464, 1995.

[11] T. Ishida et al.,"Trabecular Pattern Analysis using Fractal Dimension," *Japanese Journal of Applied Physics*, 32 Part1(4), pp. 1867-1871, 1993.

[12] National Cancer Imaging Archive (NCIA), https://imaging.nci.nih.gov/ncia/faces/baseDef.tiles